Non-Markovian dynamics of a biased qubit coupled to a structured bath

Congjun Gan, Peihao Huang and Hang Zheng

Department of Physics, Shanghai Jiao Tong University, Shanghai 200240,
People's Republic of China

E-mail: gancongjun@sjtu.edu.cn

Abstract
A new analytical approach, beyond the rotating wave approximation, based on unitary
transformations and the non-Markovian master equation for the density operator, is applied to
treat the biased spin–boson model with a Lorentzian structured bath for arbitrary detunings at
zero temperature. Compared to zero bias, we find that the non-equilibrium dynamics
demonstrates two more damping oscillation frequencies and one additional relaxation frequency
for non-zero bias. Analytical expressions for the non-Markovian dynamics and the
corresponding spectrum, the localized–delocalized transition point, the coherent–incoherent
transition point, the analytical ground energy, the renormalized tunneling factor and the
susceptibility are determined. The sum rule and the Shiba relation are checked in the coherent
regime.

(Some figures in this article are in colour only in the electronic version)

1. Introduction

In a fully quantum-mechanical way, the spin–boson model
(SBM) [1–3] is a prominent physical model in the research
of dynamics and decoherence for numerous physical and
chemical processes. Due to its advantage in the quantitative
description of quantum bits (qubits), the SBM has recently
attracted wide interest in the field of quantum computation
and information. In the last decade, many promising
scalable solid-state qubit schemes have been proposed and
realized [4–7]. Although great improvement has been made,
there are still great obstacles on the road to realizing quantum
computation and information. One of the biggest obstacles is
the decoherence of the qubits due to their coupling with the
environment [8, 9]. In SBM, the effect of the environment
is characterized by the spectral density, which is commonly
assumed to be ohmic or a power function of the bath
mode. However, in many qubit schemes realized today, the
environment of the qubit may have a certain characteristic
frequency, and consequently a shape Lorentzian peak may
appear in the spectral density [6, 7, 10–12]. For example,
the information of a flux qubit is usually read out by a
dc-SQUID with a characteristic plasma frequency. At the
same time, the environmental noise of the SQUID is also
transferred to the qubit leading to decoherence and dissipation.

A similar example is a Cooper-pare box (CPB) coupled to
a transmission line resonator. All these problems can be
modeled as a two level system (TLS) coupled to a harmonic
oscillator (HO) which itself is coupled further to a normal
ohmic environment. As an alternative but equivalent point
of view, such a qubit–HO–environment model can be exactly
mapped to the SBM with a Lorentzian structured bath $J(\omega)$
(see (6) in section 2) [13–16].

Different from the ohmic bath, the equilibrium dynamics
of the SBM with such a structured bath or the equivalent
qubit–HO–environment model have not been studied that
much. Many methods have only been studied in a particular
regime, such as the studies on a driven qubit coupled
to a structured environment by Grifoni *et al* [17, 18].
However, we are interested in a regime with static bias.
Typical studies on this particular spectral density include
the quasi-adiabatic propagator path integral (QUAPI) [19],
the van Vleck perturbation theory together with a Born–
Markov master equation (VVBM) [20], the flow equation
renormalization (FER) [21–23], the non-interacting blip
approximation (NIBA) [22, 24], an approximation scheme
by introducing a HO displacement operator [25] and a
perturbation method based on unitary transformation [26]. It is
known that QUAPI is numerical and extensive computational
resources are needed when the bath possesses a long memory

1

time [23], and we have found that QUAPI does not easily reach stable non-equilibrium dynamics for the non-zero bias case. VVBM works well with finite bias at low temperature [20]. However, VVBM uses the Van Vleck perturbation theory up to the second order in the qubit–HO coupling to get the eigenvalues and eigenfunctions of the non-dissipative qubit–HO system, solves a Born–Markov master equation for the reduced density matrix in the qubit–HO's eigenbasis, and it requires a small qubit–HO coupling and a Born–Markov approximation [20]. To our knowledge, FER has not studied non-equilibrium dynamics and needs extra setting parameters to be chosen for the best results [27]. To date, NIBA is not applicable for non-zero bias at low temperature [20, 22, 24]. Reference [25] only presents results for zero bias near resonance, meanwhile [26], with one unitary transformation also only presents results for zero bias.

In this paper, as an extension to Huang and Zheng's work [26, 28], a new analytical approach, beyond the rotating wave approximation (RWA), based on two unitary transformations and the non-Markovian master equation for the density operator, is applied to treat the biased spin–boson model (SBM) with a Lorentzian structured bath for arbitrary detunings at zero temperature. One should note that the two unitary transformations are different from [26, 28] and it makes our approach applicable both for non-zero bias and zero bias. Moreover, within a nontrivial Born approximation but without the Markovian approximation, we get the analytical density operator by the master equation method, which can be easily extended to finite temperature. Compared with [28], our approach has several advantages. First, both the localized–delocalized transition point α_L and the coherent–incoherent transition point α_c are studied; these have not been provided so far (except α_c with zero bias by [26]). Second, it works well for a wide parameter range: having no direct restriction on the qubit–HO coupling, both for biased and unbiased cases, at arbitrary finite detunings (positive/negative detunings or on resonance) and works well from weak to sufficiently strong spin–bath coupling as long as $\alpha < \alpha_c$, which is little-studied and beyond the weak coupling regime. Our results are checked in the exactly solvable special cases (such as the independent boson model and the Rabi model). The dynamics and the corresponding spectrum are compared to the literature results both for unbiased and biased cases. The Shiba relation and the sum rule have also been examined.

This paper is organized as follows. Section 2 introduces the model and our treatment. Meanwhile, the ground state energy, the renormalized tunneling factor η and localized–delocalized transition point α_L are determined. Section 3 presents the master equation and an analytical expression for the density operator without the Markovian approximation. In section 4, we have calculated the non-equilibrium dynamics $P(t)$ and the corresponding spectrum $S(\omega)$, and presented the physical interpretation. In section 5, we show the susceptibility and the validation of the Shiba relation. The coherent–incoherent transition point α_c is determined.

2. Model and treatment

In a flux qubit system, the qubit is the two macroscopically distinct quantum states representing clockwise and anticlockwise rotating supercurrents. The qubit is entangled with the detecting field, which is itself coupled with the outside noncoherent environment. The qubit can be characterized by Pauli matrices, the detecting equipment, which is actually a LC resonant circuit [6, 7], can be described by a harmonic oscillator with a characteristic frequency Ω, and the environment can be described by a set of harmonic oscillators. Therefore, the qubit–HO–environment Hamiltonian can be written as (with Planck units $\hbar = k_B = 1$):

$$H = -\frac{\Delta}{2}\sigma_x + \frac{\epsilon}{2}\sigma_z + \Omega A^\dagger A + \sum_k \omega_k a^\dagger a$$
$$+ (A^\dagger + A)\left[g\sigma_z + \sum_k \kappa_k(a_k^\dagger + a_k)\right]$$
$$+ (A^\dagger + A)^2 \sum_k \frac{\kappa_k^2}{\omega_k}, \tag{1}$$

where Δ is the energy difference of the qubit and ϵ is the applied bias; σ_x and σ_z are Pauli matrices to describe the spin system; A (or $A^\dagger$) and a_k (or $a_k^\dagger$) are the annihilation (or creation) operators of harmonic oscillators with frequencies Ω and ω_ks, respectively; g is the qubit–HO coupling and κ_k is the HO–environment coupling related to the kth oscillator. The environment is described by the ohmic spectral density $J_{\text{Ohm}}(\omega) \equiv \sum_k \kappa_k^2 \delta(\omega - \omega_k) = \Gamma\omega$, where Γ is a dimensionless coupling constant.

As an alternative but equivalent point of view, such a qubit–HO–environment model in (1) can be exactly mapped to the conventional SBM with a Lorentzian structured bath. The Hamiltonian reads [13–16, 26]

$$H = H_S + H_B + H_I, \tag{2}$$

where the subscript 'S' denotes the spin system, the subscript 'B' denotes the boson environment and the subscript 'I' denotes the interaction between the spin and the boson environment, with

$$H_S = -\frac{\Delta}{2}\sigma_x + \frac{\epsilon}{2}\sigma_z, \tag{3}$$

$$H_B = \sum_k \omega_k b_k^\dagger b_k, \tag{4}$$

$$H_I = \frac{1}{2}\sigma_z \sum_k \lambda_k(b_k^\dagger + b_k), \tag{5}$$

where $b_k^\dagger$ (b_k) is the creation (or annihilation) operator of the kth boson mode with frequency ω_k; σ_x and σ_z are Pauli matrices to describe the spin system; ϵ is the bias, Δ is the bare tunneling and λ_k is the coupling between the spin and the boson environment. We employ the symbols $|\uparrow\rangle$ and $|\downarrow\rangle$ to denote the eigenstates of the Pauli matrix σ_z with eigenvalues $+1$ and -1 respectively. The boson environment of the SBM

is described by the Lorentzian structured spectral density, and it reads [13–16]

$$J(\omega) = \sum_k \lambda_k^2 \delta(\omega - \omega_k) = \frac{2\alpha\omega\Omega^4}{(\Omega^2 - \omega^2)^2 + (2\pi\Gamma\omega\Omega)^2}, \quad (6)$$

in which $\alpha = \lim_{\omega \to 0} J(\omega)/(2\omega) = 8\Gamma g^2/\Omega^2$ is the dimensionless coupling constant.

Our treatment starts from the SBM in (2). In order to take into account the correlation between the spin and bosons, a unitary transformation is applied to H to obtain $H' = \exp(S)H\exp(-S)$, where the generator $S = \sum_k[(\lambda_k/(2\omega_k))](b_k^\dagger - b_k)[\xi_k\sigma_z + (1 - \xi_k)\sigma_0]$. Here we introduce a constant σ_0 and a k-dependent function ξ_k, which will be determined later. We rewrite the transformed $H' = H_0' + H_1' + H_2'$ as

$$H_0' = -\tfrac{1}{2}\eta\Delta\sigma_x + \tfrac{1}{2}\epsilon\sigma_z + \sum_k \omega_k b_k^\dagger b_k$$
$$- \sum_k \frac{\lambda_k^2}{4\omega_k}\xi_k(2 - \xi_k) - \sum_k \frac{\lambda_k^2}{4\omega_k}\sigma_0^2(1 - \xi_k)^2, \quad (7)$$

$$H_1' = \frac{1}{2}\sum_k \lambda_k(1 - \xi_k)(b_k^\dagger + b_k)(\sigma_z - \sigma_0) - \frac{\mathrm{i}\sigma_y}{2}\eta\Delta X, \quad (8)$$

$$H_2' = -\tfrac{1}{2}\Delta\sigma_x(\cosh X - \eta) - \tfrac{1}{2}\Delta\mathrm{i}\sigma_y(\sinh X - \eta X)$$
$$- \sum_k \frac{\lambda_k^2}{2\omega_k}\sigma_0(1 - \xi_k)^2(\sigma_z - \sigma_0), \quad (9)$$

where $X \equiv \sum_k(\lambda_k\xi_k/\omega_k)(b_k^\dagger - b_k)$, and η is the thermodynamic average of $\cosh X$, as

$$\eta = Z^{-1}\mathrm{Tr}[\exp(-\beta H)\cosh X]$$
$$= \exp\left[-\sum_k \frac{\lambda_k^2}{2\omega_k^2}\xi_k^2 \coth\left(\frac{\omega_k}{2T}\right)\right], \quad (10)$$

where $Z = \mathrm{Tr}[\exp(-\beta H)]$ and $T = 1/\beta$ is the temperature.

Since the spin and bosons are decoupled in H_0', it is exactly solvable, by a unitary matrix $U = \begin{pmatrix} u & v \\ v & -u \end{pmatrix}$, with $u = \sqrt{(1 - \epsilon/W)/2}$, $v = \sqrt{(1 + \epsilon/W)/2}$ and $W = \sqrt{\epsilon^2 + \eta^2\Delta^2}$. The unitary matrix U only acts on the spin operators, such as σ_x and σ_z. The diagonalized $\tilde{H}_0 = U^\dagger H_0'U$ reads[1].

$$\tilde{H}_0 = -\tfrac{1}{2}W\tilde{\sigma}_z + \sum_k \omega_k b_k^\dagger b_k$$
$$- \sum_k \frac{\lambda_k^2}{4\omega_k}\xi_k(2 - \xi_k) - \sum_k \frac{\lambda_k^2}{4\omega_k}\sigma_0^2(1 - \xi_k)^2, \quad (11)$$

where $\tilde{\sigma}_{x,y,z}$ are the Pauli matrices after the U unitary transformation. Here, we employ the symbols $|\pm\rangle$ to denote the eigenstates of the Pauli matrix $\tilde{\sigma}_z$ with eigenvalues ±1 respectively. The eigenstate of $\tilde{H}_0$ is the direct product $|\{n_k\}, \pm\rangle$, where $|\{n_k\}\rangle$ are the eigenstates of bosons with n_k phonons for the mode k. The ground state of $\tilde{H}_0$ is $|g_0\rangle = |\{0_k\}, +\rangle$ and the lowest exited states are $|\{0_k\}, -\rangle$, $|\{1_k\}, +\rangle$ and $|\{1_k\}, -\rangle$.

---

[1] Mathematically, the transformation should extend to the Hilbert space of the spin–boson system by denoting U to the direct product with 1_B as $U \otimes 1_B$, where 1_B is the identity matrix of the Hilbert space of the boson environment. In the operator level, it is convenient to omit the extension.

Similarly, we make the transformations to get $\tilde{H}_1 = U^\dagger H_1'U$ and $\tilde{H}_2 = U^\dagger H_2'U$, which are treated as perturbations and should be as small as possible. For this purpose, it is determined as $\sigma_0 = -\epsilon/W$ and $\xi_k = \omega_k/(\omega_k + W)$. Thus

$$\tilde{H}_1 = \tfrac{1}{2}(1 - \tilde{\sigma}_z)\sum_k Q_k(b_k^\dagger + b_k)$$
$$+ \tfrac{1}{2}\sum_k V_k[b_k^\dagger(\tilde{\sigma}_x + \mathrm{i}\tilde{\sigma}_y) + b_k(\tilde{\sigma}_x - \mathrm{i}\tilde{\sigma}_y)], \quad (12)$$

where $Q_k = \lambda_k[\epsilon/(\omega_k + W)]$ and $V_k = \lambda_k[\eta\Delta/(\omega_k + W)]$. In the SBM, $\lambda_k \ll \Delta$. Q_k and V_k can be viewed as the renormalized spin–bath coupling, and they are always smaller than λ_k and even smaller for high frequencies. Obviously, $\tilde{H}_1|g_0\rangle = 0$. Under the eigenbasis of $\tilde{H}_0$, $\tilde{H}_1$ has only off-diagonal terms and, in the lowest states, it is $\langle\{0_k\}, -|\tilde{H}_1|\{1_k\}, +\rangle = V_k$, $\langle\{0_k\}, -|\tilde{H}_1|\{1_k\}, -\rangle = Q_k$ and $\langle\{1_k\}, -|\tilde{H}_1|\{1_{k'}\}, +\rangle = 0$. Meanwhile, the terms in $\tilde{H}_2$ are related to the multi-boson transition, and their contributions to the physical quantities are to the fourth order of λ_k ($\mathrm{O}(\lambda_k^4)$). These are key points in our approach. The transformed Hamiltonian is approximated as

$$\tilde{H} = \tilde{H}_0 + \tilde{H}_1 + \tilde{H}_2 \approx \tilde{H}_0 + \tilde{H}_1 \quad (13)$$

in the following. Note that the treatment above is an extension to the one proposed by [28], while our generator S and the second unitary transformation are different. However, the k-dependent function ξ_k and decomposing the Hamiltonian into three parts are done with the same spirit and they have been discussed in detail in [28].

Thus, the ground energy of $\tilde{H}$ is just the same as that of $\tilde{H}_0$, and it is determined as

$$E_g = -\frac{1}{2}W - \sum_k \frac{\lambda_k^2}{4\omega_k}\left[1 - \left(\frac{\eta\Delta}{\omega_k + W}\right)^2\right]. \quad (14)$$

The Hamiltonian H in (2) can be solved exactly in two limits: one is the weak coupling limit with $E_g(\alpha \to 0) = -\sqrt{\Delta^2 + \epsilon^2}/2$ and the other is the zero tunneling limit (the independent boson model) with $E_g(\Delta \to 0) = -|\epsilon|/2 - \sum_k \lambda_k^2/(4\omega_k)$. The ground energies in (14) are the same in both limits.

Up to now, the deduction is independent of any specific spectral density and it is not restricted to zero temperature. In the following, the treatment is at zero temperature. As shown in H_0', η is the renormalized tunneling factor. In the limit of zero temperature, it is

$$\eta = \exp\left[-\int_0^\infty \frac{J(\omega)\,\mathrm{d}\omega}{2(\omega + W)^2}\right]. \quad (15)$$

The integration in (15) can be done to the end, analytically. In the case of zero bias ($\epsilon = 0$), η has the same expression as Huang's and a similarly positive change of the tunneling frequency can be predicted when $\Delta \sim \Omega$, which fails in the adiabatic approach [26]. Generally, the renormalized tunneling factor η is larger than 0, which means that there is an effective tunneling between the two states of the qubit in a realistic situation. If the renormalized tunneling factor suddenly changes to 0, the localized–delocalized transition occurs and the qubit will be localized in one of the two states where it was located before the transition.
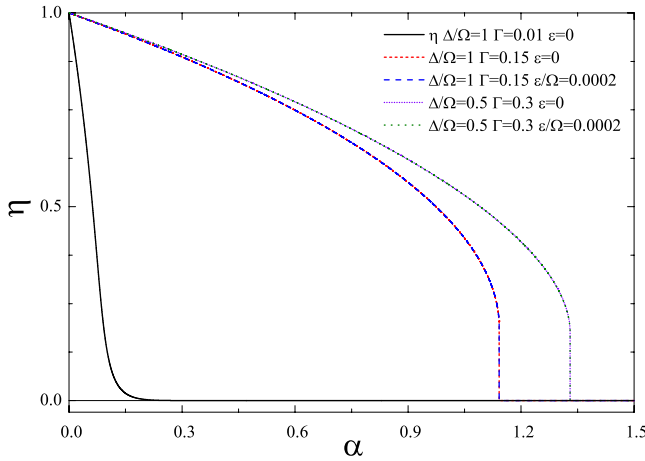
Figure 1. The renormalized tunneling factor η versus α. It shows that η goes to zero gradually with smaller Γ and it goes to zero suddenly with larger Γ.

Figure 2. Phase diagram of the localized–delocalized transition point α_L versus ϵ. It shows that α_L is almost the same with different Δ and the curve changes rapidly for larger Γ and/or smaller ϵ. Parameters: near resonance $\Delta = \Omega$, $\Gamma = 0.01, 0.02, 0.05, 0.1$; off resonance $\Delta = 0.5\Omega$, $\Gamma = 0.01, 0.02, 0.05, 0.1$.

Figure 1 shows numerical results of η as a function of α. For larger Γ (e.g. 0.15, 0.3), one can see that η suddenly goes to zero at the localized–delocalized transition point $\alpha = \alpha_L$, where $\eta = 0$ for all $\alpha \geqslant \alpha_L$. While for smaller Γ (e.g. 0.01), η gradually goes to zero, and we set the cut at the value $\eta = 0.0001$, which is small enough.

A phase diagram of the delocalized–localized transition point α_L versus bias ϵ is plotted in figure 2 with different Γ (=0.01, 0.02, 0.05, 0.1) and different detunings Δ/Ω (=0.5, 1). The area of $\alpha < \alpha_L$ is called the 'localized phase', and the area of $\alpha > \alpha_L$ the 'delocalized phase'. It shows that α_L increases with increasing ϵ and it is almost the same for different Δs. The change of α_L is more significant for larger Γ or smaller ϵ.

3. Density operator and master equation

In the Schrödinger picture, the density operator of the SBM is denoted as $\rho_{SB}(t)$ for the Hamiltonian H in (2), and the density operator for $\tilde{H}$ in (13) is $\tilde{\rho}_{SB}(t) = U^\dagger \exp(S)\rho_{SB}(t)\exp(-S)U$, where the subscript 'SB' denotes the total spin–boson system. In the following, it will be analyzed in the interaction picture, denoted by a superscript 'I' in the operator. $\tilde{H}_0$ is treated as the unperturbed part and $\tilde{H}_1$ as a perturbation. Moreover, in the interaction picture, it is assumed that the density operator for $\tilde{H}$ is $\tilde{\rho}_{SB}^I(t) = \tilde{\rho}_S^I(t)\rho_B$, where $\tilde{\rho}_S^I(t) = \mathrm{Tr}_B\,\tilde{\rho}_{SB}^I(t)$ is the reduced density operator. Within the Born approximation (only keeping the second order of $\tilde{H}_1$), we can obtain the non-Markovian master equation for the reduced density operator

$$\frac{\mathrm{d}}{\mathrm{d}t}\tilde{\rho}_S^I(t) = -\int_0^t \mathrm{Tr}_B[\tilde{H}_1(t), [\tilde{H}_1(t'), \tilde{\rho}_S^I(t')\rho_B]]\,\mathrm{d}t', \quad (16)$$

where $\tilde{H}_1(t)$ is denoted as the perturbed part $\tilde{H}_1$ in the interaction picture. Since the renormalized spin–bath coupling Q_k and V_k in $\tilde{H}_1$ are always smaller than λ_k, it makes our Born approximation nontrivial and more reasonable by comparing it
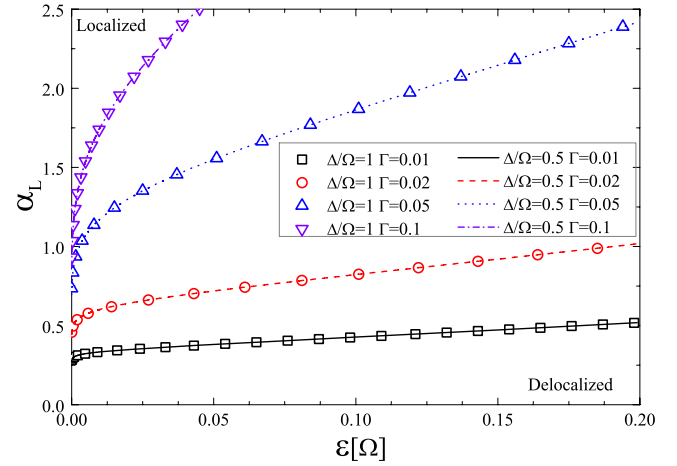
with the commonly used Born approximation [29, 30], which directly does the perturbation to the second order of H_I in (2).

The master equation in (16), without the Markovian approximation, can be done to the end with a Laplace transformation and an inverse-Laplace transformation. Changing from the interaction picture back to the Schrödinger picture, denoting the reduced density operator in the Schrödinger picture as $\tilde{\rho}_S(t) = \begin{pmatrix} \tilde{\rho}_{11}(t) & \tilde{\rho}_{12}(t) \\ \tilde{\rho}_{21}(t) & \tilde{\rho}_{22}(t) \end{pmatrix}$ for $\tilde{H}$, at zero temperature, we obtain

$$\tilde{\rho}_{21}(t) = \frac{\tilde{\rho}_{21}(0)}{2\pi}\int_{-\infty}^\infty \frac{\mathrm{i}\exp(-\mathrm{i}\omega t)\,\mathrm{d}\omega}{\omega - W - \Sigma(\omega) + \mathrm{i}\Gamma(\omega)}, \quad (17)$$

and

$$\tilde{\rho}_{22}(t) = \frac{\tilde{\rho}_{22}(0)}{2\pi}\int_{-\infty}^\infty \frac{\mathrm{i}\exp(-\mathrm{i}\omega t)\,\mathrm{d}\omega}{\omega - \Sigma'(\omega) + \mathrm{i}\Gamma'(\omega)}. \quad (18)$$

Abbreviations are used in (17) and (18), as

$$\Gamma(\omega) = \gamma(\omega) + \frac{\epsilon^2}{\eta^2\Delta^2}\gamma(\omega - W), \quad (19)$$

$$\Sigma(\omega) = R(\omega) + \frac{\epsilon^2}{\eta^2\Delta^2}R(\omega - W), \quad (20)$$

and

$$\Gamma'(\omega) = \gamma(W + \omega) + \gamma(W - \omega), \quad (21)$$

$$\Sigma'(\omega) = R(W + \omega) - R(W - \omega), \quad (22)$$

where $R(\omega)$ and $\gamma(\omega)$ are the real and imaginary parts of $\sum_k V_k^2/(\omega - \mathrm{i}0^+ - \omega_k)$ (0^+ is a positive infinitesimal introduced by the inverse-Laplace transformation).

$$R(\omega) = \sum_{\mathbf{k}} \frac{V_k^2}{(\omega - \omega_{\mathbf{k}})} = \int_0^\infty \frac{\eta^2\Delta^2 J(\omega')\,\mathrm{d}\omega'}{(\omega - \omega')(\omega' + W)^2}, \quad (23)$$

$$\gamma(\omega) = \pi\sum_{\mathbf{k}} V_k^2\delta(\omega - \omega_{\mathbf{k}}) = \frac{\pi\eta^2\Delta^2 J(\omega)}{(\omega + W)^2}, \quad (24)$$

respectively. In addition, two other terms in $\tilde{\rho}_S(t)$ are $\tilde{\rho}_{12}(t) = [\tilde{\rho}_{21}(t)]^\dagger$ and $\tilde{\rho}_{11}(t) = 1 - \tilde{\rho}_{22}(t)$. Since the specific form of $J(\omega)$ is not involved an analytical expression of the reduced density operator $\tilde{\rho}_S(t)$ is offered and it is independent of any specific spectral density.

We assume the initial density operator at $t = 0$ is $\rho_{SB}(0) = \exp(-S)[|\uparrow\rangle\langle\uparrow| \otimes \rho_B(0)]\exp(S)$, where the spin is in the lower state $|\uparrow\rangle\langle\uparrow|$ and $\rho_B(0)$ is the equilibrium state. Thus, the corresponding initial reduced density operator for $\tilde{H}$ in (13) is

$$\tilde{\rho}_S(0) = \frac{1}{2}\begin{pmatrix} 1 - \epsilon/W & \eta\Delta/W \\ \eta\Delta/W & 1 + \epsilon/W \end{pmatrix}. \qquad (25)$$

4. Non-equilibrium dynamics and the physical interpretation

For the SBM, it is common to evaluate the non-equilibrium dynamics $P(t)$, as this is the quantity of interest in the experiments. $P(t)$ is also called the population difference. Following the unitary transforms, it is determined as

$$\begin{aligned} P(t) &= \text{Tr}_S(\text{Tr}_B(\rho_{SB}(t)\sigma_z)) \\ &= \text{Tr}_S(\text{Tr}_B(\exp(-S)U\tilde{\rho}_{SB}(t)U^\dagger\exp(S)\sigma_z)) \\ &= \frac{\epsilon}{W}[2\tilde{\rho}_{22}(t) - 1] + \frac{2\eta\Delta}{W}\text{Re}[\tilde{\rho}_{21}(t)]. \end{aligned} \qquad (26)$$

Substituting (17) and (18) into (26) with the initial condition in (25), the dynamics read

$$\begin{aligned} P(t) &= \frac{2\epsilon}{\pi W}\left(1 + \frac{\epsilon}{W}\right)\int_0^\infty d\omega \frac{\cos(\omega t)\Gamma'(\omega)}{[\omega - \Sigma'(\omega)]^2 + [\Gamma'(\omega)]^2} \\ &+ \frac{\eta^2\Delta^2}{\pi W^2}\int_0^\infty d\omega \frac{\cos(\omega t)\Gamma(\omega)}{[\omega - W - \Sigma(\omega)]^2 + [\Gamma(\omega)]^2} - \frac{\epsilon}{W}. \end{aligned} \qquad (27)$$

Thus, we end up with an exact analytical expression of the non-Markovian dynamics $P(t)$ in (27). As time goes to infinity, we have the dynamics at the long time limit $P(t \to \infty) = -\epsilon/W$.

4.1. Spectrum of the non-Markovian dynamics

In order to get insight into the dominant frequencies of $P(t)$, a Fourier transform is applied to (27) according to

$$S(\omega) \equiv \int_{-\infty}^\infty dt \cos(\omega t) P(t). \qquad (28)$$

The spectrum $S(\omega)$ is an even function and for $\omega \geqslant 0$ it is written as

$$\begin{aligned} S(\omega) &= \frac{2\epsilon}{W}\left(1 + \frac{\epsilon}{W}\right)\frac{\Gamma'(\omega)}{[\omega - \Sigma'(\omega)]^2 + [\Gamma'(\omega)]^2} \\ &+ \frac{\eta^2\Delta^2}{W^2}\frac{\Gamma(\omega)}{[\omega - W - \Sigma(\omega)]^2 + [\Gamma(\omega)]^2} - \frac{2\pi\epsilon}{W}\delta(\omega). \end{aligned} \qquad (29)$$

The frequency property of the dynamics $P(t)$ can be analyzed directly by $S(\omega)$. On one hand, the first two terms in (29) are Lorentzian-like functions. On the other hand, $\gamma(\omega)$ is small when g is small or ω is away from Ω, thus $\Gamma(\omega)$ and $\Gamma'(\omega)$, which are functions related to $\gamma(\omega)$, are usually small. Therefore, the dominant frequencies of $S(\omega)$ should be the solutions ω_p of the equation

$$\omega - W - \Sigma(\omega) = 0, \qquad (30)$$

and the solutions $\omega_{p'}$ of the equation

$$\omega - \Sigma'(\omega) = 0. \qquad (31)$$

Since the dissipative environment generally adds a shift and width to the dominant frequencies, we can investigate the physical nature in the limit of small HO–environment coupling ($\Gamma \to 0$). Consequently, the spectral density $J(\omega)$ in (6) goes to $(4g^2\Omega/\omega)[\delta(\omega - \Omega) + \delta(\omega + \Omega)]$ and $R(\omega)$ in (23) goes to $4g^2\eta^2\Delta^2/[(\omega - \Omega)(\Omega + W)^2]$. Therefore, according to (30) and (20), the dominant frequencies ω_p are the solutions of the equation

$$\omega - W = \frac{4g^2}{(\Omega + W)^2}\left[\frac{\eta^2\Delta^2}{\omega - \Omega} + \frac{\epsilon^2}{\omega - \Omega - W}\right]. \qquad (32)$$

Equation (32) can be solved exactly. If $g^2\epsilon^2/[\Delta^2(\Omega + W)^2] \ll 1$, ω_p can be simplified and approximated as

$$\omega_{p1,2} \cong \frac{\Omega + W}{2} \pm \sqrt{\left(\frac{\Omega - W}{2}\right)^2 + \frac{4g^2\eta^2\Delta^2}{(\Omega + W)^2}}, \qquad (33)$$

where the subscripts '1, 2' relate to the sign '+, −', respectively, and

$$\omega_{p3} \cong (\Omega + W) + \frac{W4g^2\epsilon^2}{\Omega W(\Omega + W)^2 - 4g^2\eta^2\Delta^2}. \qquad (34)$$

Similarly, according to (31) and (22), the dominant frequencies $\omega_{p'}$ are exactly solvable as

$$\omega_{p'1} = 0 \qquad (35)$$

and

$$\omega_{p'2,3} = \pm\sqrt{(W - \Omega)^2 + \frac{8g^2\eta^2\Delta^2}{(\Omega + W)^2}}. \qquad (36)$$

Since $S(\omega)$ is an even function, we only need to consider the non-negative part ($\omega \geqslant 0$). Thus, the negative one ($\omega_{p'3}$) of the solutions $\omega_{p'}$ in (36) is discarded. Consequently, for non-zero bias, there are five dominant frequencies: $\omega_{p'1} = 0$, $\omega_{p'2}$, ω_{p1}, ω_{p2}, ω_{p3}.

For zero bias ($\epsilon = 0$), we have $\Gamma(\omega) = \gamma(\omega)$, $\Sigma(\omega) = R(\omega)$ and

$$S(\omega) = \frac{\eta^2\Delta^2}{W^2}\frac{\Gamma(\omega)}{[\omega - W - R(\omega)]^2 + [\gamma(\omega)]^2} \qquad (37)$$

for the non-negative part $\omega \geqslant 0$. Similarly, the dominant frequencies can be determined, but with only two frequencies ω_{p1} and ω_{p2}, which are the exactly solvable solutions of $\omega - W - R(\omega) = 0$, as

$$\omega_{p1,2} = \frac{\Omega + W}{2} \pm \sqrt{\left(\frac{\Omega - W}{2}\right)^2 + \frac{4g^2\eta^2\Delta^2}{(\Omega + W)^2}}. \qquad (38)$$

It is consistent with Huang's results (see equation (17) in [26]). Compared to unbiased case, the effect of finite bias leads to three additional dominant frequencies: $\omega_{p'1} = 0$, $\omega_{p'2}$, ω_{p3}.

Since the renormalized tunneling in the limit of small HO–environment coupling is

$$\eta = \exp\left[-\frac{2g^2}{(\Omega + W)^2}\right] \cong 1, \qquad (39)$$

the resonance condition is $\Omega = W_0 = \sqrt{\Delta^2 + \epsilon^2} \cong W$. For the near resonance $\Omega = W$ case, equation (33) can be simplified and approximated as

$$\omega_{p1,2} \cong \Omega \pm \frac{\eta\Delta}{\Omega}g. \qquad (40)$$

For zero bias, there are only two dominant frequencies $\omega_{p1,2} = \Omega \pm g$ according to (38), which is consistent with the result of the simple exactly solvable Jaynes–Cummings model [31]. Moreover, for $\Omega = W$ with finite bias (36) can be simplified as

$$\omega_{p'2} = \frac{\sqrt{2}\eta\Delta}{\Omega}g. \qquad (41)$$

In the case of finite detunings $|\Omega - W| > 0$, with small qubit–HO coupling $g \ll \Delta$, Ω, (33) and (36) can be simplified and approximated as

$$\omega_{p1,2} \cong W + \frac{4g^2\eta^2\Delta^2}{(W - \Omega)(\Omega + W)^2} \qquad (42)$$

or

$$\Omega + \frac{4g^2\eta^2\Delta^2}{(\Omega - W)(\Omega + W)^2}, \qquad (43)$$

(in (42) and (43), the larger one is ω_{p1} and vice versa) and

$$\omega_{p'2} \cong |W - \Omega| + \frac{4g^2\eta^2\Delta^2}{|W - \Omega|(\Omega + W)^2}. \qquad (44)$$

One can clearly show the physics of all these dominant frequencies: $\omega_{p'1} = 0$ (35) is a relaxation peak, ω_{p1} and ω_{p2} are related to the renormalized energy difference of the qubit in (42) and the energy of the HO in (43), and $\omega_{p'2}$ is related to the energy difference of the qubit and the HO in (44). Meanwhile, ω_{p3} is related to the summation of the qubit energy W and the HO energy Ω as shown in (34). Therefore, for small qubit–HO coupling, due to the dressing of the boson bath, ω_{p3} and $\omega_{p'2}$ are not exactly the summation or the difference between W and Ω, however, we might still call $\omega_{p'2}$ the 'beat frequency' and ω_{p3} the 'sum frequency'.

4.2. Spectrum of the qubit–HO system

Before exploring the exact spectrum $S(\omega)$ corresponding to the non-Markovian $P(t)$ in a realistic situation, as an alternative view to (2), we will briefly investigate the energy spectrum of the equivalent qubit–HO–environment model (1), which is a physically clearer way. Since the environment generally shifts and broadens the spectrum, to get a rough idea, the qubit–HO–environment model without HO–environment coupling ($\Gamma =$

0) is investigated here, and the qubit–HO Hamiltonian reads (so-called Rabi model)

$$H_{q-HO} = -\frac{\Delta}{2}\sigma_x + \frac{\epsilon}{2}\sigma_z + \Omega A^\dagger A + (A^\dagger + A)g\sigma_z. \qquad (45)$$

If the qubit–HO is decoupled ($g = 0$), (45) is exactly solvable. By applying a unitary matrix to H_{q-HO}, it can be diagonalized as

$$H_{q-HO} = -\frac{W_0}{2}\breve{\sigma}_z + \Omega A^\dagger A, \qquad (46)$$

where $W_0 = \sqrt{\epsilon^2 + \Delta^2}$. Thus, the spectrum of the decoupled qubit–HO without environment is exactly shown, with eigenbasis $|n, \breve{\pm}\rangle$, where $|n\rangle$ denotes the eigenstates of HO with n ($n = 0, 1, \ldots, \infty$) phonons and $|\breve{\pm}\rangle$ denotes the eigenstates of the Pauli matrix $\breve{\sigma}_z$ with eigenvalues ± 1 respectively.

If the qubit–HO is switched on ($g \neq 0$), (45) can be solved with exact numerical diagonalization, with an eigenbasis denoted as $|j\rangle$ ($j = 0, 1, \ldots, \infty$), which has been ordered increasingly according to the eigenenergies.

To further explore the instinct of the coupled qubit–HO system, an analytical deduction beyond RWA is provided as follows. Since (45) has a similar form to (2) when removing the summation and the multimode index k and substituting $\omega_k \to \Omega$, $b_k^\dagger \to A^\dagger$, $b_k \to A$ and $\lambda_k/2 \to g$ we, therefore, make two similar unitary transformations $U'^\dagger \exp(S')H \exp(-S')U'$ to H in (45) with generator $S' = (g/\Omega)(A^\dagger - A)[\Omega\sigma_z/(\Omega + W') - \epsilon/(\Omega + W')]$ and $U' = \begin{pmatrix} u' & v' \\ v' & -u' \end{pmatrix}$, with $u' = \sqrt{(1 - \epsilon/W')/2}$, $v' = \sqrt{(1 + \epsilon/W')/2}$ and $W' = \sqrt{\epsilon^2 + \eta'^2\Delta^2}$, and to the second order of the qubit–HO coupling g ($O(g^2)$), it results in

$$H_{q-HO} \cong -\frac{1}{2}W'\tilde{\sigma}_z' + \Omega A^\dagger A + \frac{\epsilon g}{\Omega + W'}(1 - \tilde{\sigma}_z')(A^\dagger + A)$$
$$+ \frac{\eta'\Delta g}{\Omega + W'}[A^\dagger(\tilde{\sigma}_x' + i\tilde{\sigma}_y') + A(\tilde{\sigma}_x' - i\tilde{\sigma}_y')]$$
$$- \frac{g^2(\Omega + 2W')}{(\Omega + W')^2} - \frac{g^2\epsilon^2}{\Omega(\Omega + W')^2}, \qquad (47)$$

where $\eta' = \exp[-2g^2/(\Omega + W')^2]$. Note that $(1 - \tilde{\sigma}_z')|+\rangle' = 0$, where $|+\rangle'$ denotes the eigenstate of the Pauli matrix $\tilde{\sigma}_z'$ with eigenvalue $+1$. If the value $|\epsilon g/[\Delta(\Omega + W')]| \ll 1$, then the term $\epsilon g(1 - \tilde{\sigma}_z')(A^\dagger + A)/(\Omega + W')$ in (47) can be discarded. Therefore, H_{q-HO} is exactly solvable analytically.

For zero bias, ($\epsilon = 0$) [20] has used the Van Vleck perturbation up to the second order g and solved a Born–Markov master equation in the system's eigenbasis to get the dynamics $P(t) = \sum_n p_{nn}(t) + \sum_{n,m(n>m)} p_{nm}(t)$ with the phonon number n, $m = 0, 1, \ldots \infty$, and proposes selection rules for zero bias: $p_{nn}(t)$ vanishes for any n, and the non-zero $p_{nm}(t)$ only exists for three cases: $|n_{\text{even}} - m_{\text{even}}| = 2$, $|n_{\text{odd}} - m_{\text{odd}}| = 2$, $n_{\text{even}} - m_{\text{odd}} = 3$ or $n_{\text{odd}} - m_{\text{even}} = 1$. When substituting $\epsilon = 0$ into (47), the Hamiltonian (47) is exactly solvable analytically. Following [20], the selection rules can be deduced similarly. The selection rules show that the transition between the lowest energy levels $|j\rangle$: $|0\rangle \leftrightarrow |1\rangle$ and $|0\rangle \leftrightarrow |2\rangle$ are allowed, whereas $|1\rangle \leftrightarrow |2\rangle$ and $|0\rangle \leftrightarrow |3\rangle$ are forbidden. This offers a second way to explain why there are only two dominant frequencies for zero bias.

4.3. The numerical ab initio technique QUAPI

In order to make comparisons with the results from the exact numerical method, we have applied the iterative tensor multiplication scheme derived for the so-called QUAPI. The numerical method was developed by Makri and Makarov [32–34]. It can be used both for the zero bias and non-zero bias open quantum systems. Reference [19] has already employed the QUAPI method to calculate the spectrum of the symmetrized correlation function of the qubit–HO–environment system with memory length $\Delta k_{max} = 1$ (checked at $\Delta k_{max} = 2$). The starting Hamiltonian of the QUAPI is (1). Our environment is the ohmic bath, which is the same as that in [33], however, our system is the qubit–HO system, which is rather complicated. Similarly, we map the QUAPI method for the non-equilibrium dynamics with similar steps, and *the parameters have exactly the same symbols as used in* [33].

(i) The first parameter is the dimension N_d of the Hilbert space of the qubit–HO system. The Hamiltonian of the qubit–HO system can be numerically diagonalized in the N_d dimension of the Hilbert space. Meanwhile, we have employed a second parameter M, which is the lowest energy sub-space of the dimension N_d of the Hilbert space of the qubit–HO system. Thus, we can diagonalize the qubit–HO space in the larger dimension N_d of the Hilbert space, to get more accurate low energy eigenstates and calculate the physical quantities in the M dimension subspace with less numerical computation. Here we should choose larger M for stronger qubit–HO coupling g.

(ii) The second parameter is the memory length Δk_{max} in the influence function. If $\Delta k_{max} \leqslant 1$, the dynamics in this approximation are Markovian. If the nonlocality extends over longer time, terms with $\Delta k_{max} > 1$ will have to be included to obtain accurate results. Comparing to [33] for the SBM problem with the ohmic bath, only $\Delta k_{max} = 5, 7$ reaches stability for zero bias (as shown in figure 2 in [33]) and only $\Delta k_{max} = 7, 9$ reaches the long time limit for non-zero bias (as shown in figure 5 in [33]). Since our system is complicated, we should use at least $\Delta k_{max} \geqslant 7, 9$ to show a stable long time limit for the non-zero bias case.

(iii) The third parameter time-step Δt is used to propagate the propagator tensor $A^{(\Delta k_{max})}$, which is a vector of dimension $(M^2)^{(\Delta k_{max})}$, and the corresponding tensor propagator $T^{(2\Delta k_{max})}$ is a matrix of dimension $(M^2)^{(2\Delta k_{max})}$. The memory time of the non-Markovian steps used by QUAPI is $\Delta k_{max} \Delta t$. The stability of the iterative density matrix propagation ensures the choices of Δt (it should not be too big nor too small). Therefore, we could choose appropriate Δt to reach larger non-Markovian memory time under this stability.

In the following numerical calculation by QUAPI, we have checked for $g \leqslant 0.5\Delta$: $N_d = 100$ is good enough, and $M \geqslant 6$ is the minimal requisite to demonstrate the dynamics qualitatively. For zero bias with weak $g \leqslant 0.18\Delta$, $\Delta k_{max} = 1$ could demonstrate the dynamics qualitatively. However, for non-zero bias, $\Delta k_{max} = 3$ is still not stable. The most time-consuming process is the calculation of the propagator tensor $A^{(\Delta k_{max})}$, requiring $(M^2)^{(2\Delta k_{max})}$ loops, which is beyond our computational resources for $M \geqslant 6$ and $\Delta k_{max} \geqslant 4$.
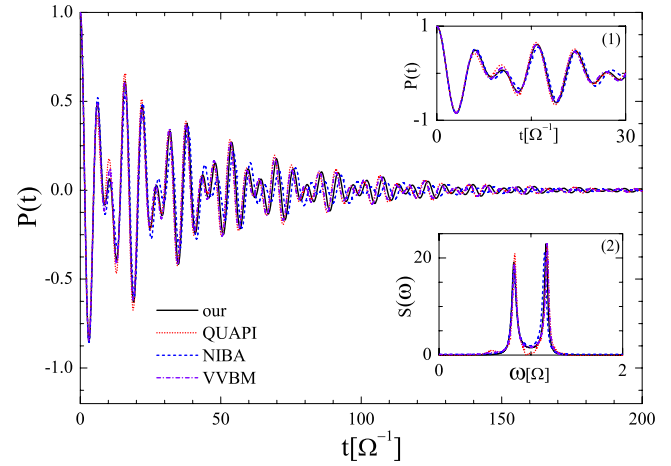

Figure 3. For zero bias ($\epsilon = 0$), non-Markovian dynamics $P(t)$ and its corresponding spectrum $S(\omega)$ at zero temperature show good agreement with results by QUAPI at zero temperature, and by NIBA [24] and VVBM [20] at low temperature $T = 0.1\Delta$. Inset (1) is a magnified part and inset (2) shows $S(\omega)$ versus ω. Parameters: $\Delta = \Omega$, $g = 0.18\Delta$, $\alpha = 0.004$, $\Gamma = 0.0154$. Parameters for QUAPI, $\Delta k_{max} = 1$, $\Delta t = 0.4/\Delta$, $N_d = 100$, $M = 30$.

4.4. Results and discussion

The Markovian approximation of $P(t)$ is equivalent to approximating the integration in (17) and (18) by the residue theorem with single pole at $-2i\gamma_0$ and $\omega_0 - i\gamma_0$, respectively. It leads to

$$P(t) = \frac{\eta^2 \Delta^2}{W^2} \cos(\omega_0 t) \exp(-\gamma_0 t)$$
$$+ \frac{\epsilon}{W} \left[\left(\frac{\epsilon}{W} + 1 \right) \exp(-2\gamma_0 t) - 1 \right], \tag{48}$$

where $\gamma_0 = \gamma(W)$ is the Weisskopf–Wigner approximation for the decay rate and $\omega_0 = W + \Sigma(W)$ ($\Sigma(W)$ is the level shift). In the long time limit, the Markovian dynamics are the same as the non-Markovian ones.

In figure 3, in the case of zero bias ($\epsilon = 0$) with weak coupling ($\Delta = \Omega$, $g = 0.18\Omega$, $\alpha = 0.004$, $\Gamma = 0.0154$), our non-Markovian dynamics $P(t)$ and the corresponding spectrum $S(\omega)$ at zero temperature is compared with the ones by VVBM [20] (the numerical results) and by NIBA [24] at low temperature $T = 0.1\Delta$. We have also checked the results by QUAPI at zero temperature with $\Delta k_{max} = 1$, $\Delta t = 0.4/\Delta$, $N_d = 100$, $M = 30$. They have shown good agreement with both $P(t)$ and $S(\omega)$. The reasons for comparing to other results at low temperature are: first, corresponding results at zero temperature by other methods are not found in the literature; second, the temperature gives a factor $\coth(\frac{\omega}{2T})$ for each frequency, and in a rough view $\coth(\frac{\omega}{2T}) \sim 1$ for typical frequencies (e.g. $\omega = \Delta$) at $T = 0.1\Delta$; third, the temperature $T = 0.1\Delta$ is low and the comparisons show that their properties are similar.

From figures 4 to 6, at finite bias ($\epsilon = -0.5\Delta$, $g = 0.18\Delta$, $\Gamma = 0.0154$), our non-Markovian dynamics $P(t)$ and the corresponding spectra $S(\omega)$ at zero temperature are compared with the numerical results by VVBM [20] at low temperature $T = 0.1\Delta$ for three different situations: the qubit being at
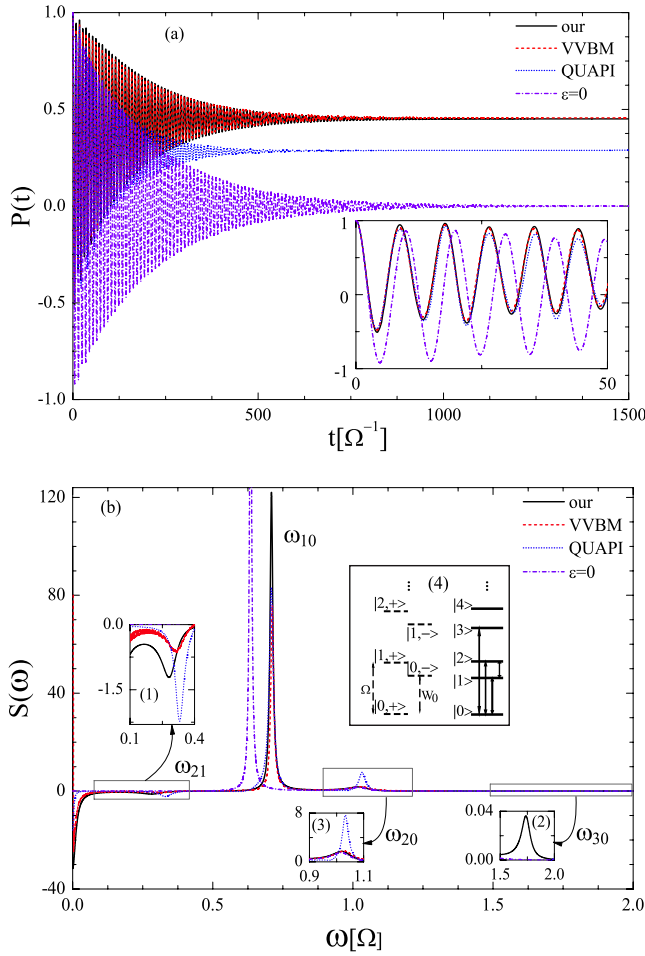
Figure 4. For off resonance $\Omega = 1.5\Delta$ with $\epsilon = -0.5\Delta$, (a) non-Markovian dynamics $P(t)$ and (b) its corresponding spectrum $S(\omega)$ at zero temperature shows qualitative agreement with VVBM [20] at low temperature $T = 0.1\Delta$. In detail, our spectrum presents one relaxation dip (at $\omega = 0$), one dephasing dip (ω_{21}) and three dephasing peaks (ω_{10}, ω_{20}, ω_{30}). Moreover, the height of our peak at ω_{10} and our dip at ω_{21} is nearly twice those by VVBM. For zero bias, there are only two dephasing peaks. Insets: the inset in (a) and insets (1)–(3) in (b) present magnified views. Inset (4) in (b) presents the schematic energy levels of the qubit–HO system with finite bias, where the dashed lines in the left part are for the uncoupled case ($g = 0$) and the solid lines in the right part are numerically exact results for the coupled case. Our dominant frequencies are related to the energy differences of the coupled qubit–HO system with numerical calculation. Parameters: $g = 0.18\Delta$, $\Gamma = 0.0154$, $\alpha = 0.001\,77$. As additional proof, the results QUAPI at zero temperature are also provided with parameters $\Delta k_{\max} = 2$, $\Delta t = 0.3/\Delta$, $N_d = 100$, $M = 10$; however, these are not stable results due to the restriction of our computation resources.

positive detunings with the HO ($\Omega = 1.5\Delta > W_0$), on resonance at ($\Omega = W_0$), and negative detunings with ($\Omega = 0.9\Delta < W_0$). Both the dynamics and the spectra have shown agreement. Moreover, *our spectrum presents five dominant frequencies*: one relaxation dip (at $\omega = 0$), one dephasing dip (ω_{21}) and three dephasing peaks (ω_{10}, ω_{20}, ω_{30}), where the four damping oscillation frequencies are related to the energy differences of the four lowest energy levels of the coupled qubit–HO system, as shown in the insets, and they have been

verified by the exact numerical diagonalization of H_{q-HO} (45). Note that the symbols ω_{ij} denote the dominant frequencies of $S(\omega)$ relating to the energy difference of the energy levels $|i\rangle$ and $|j\rangle$ of the coupled qubit–HO system ($|i\rangle$ and $|j\rangle$ are eigenstates of the qubit–HO system, as denoted in section 4.2). Meanwhile, the dominant frequencies can also be interpreted well with the relaxation dip at $\omega = 0 \Leftrightarrow \omega_{p'1} = 0$ in (35), the dephasing peaks at $\omega_{10} \Leftrightarrow \omega_{p2}$ and $\omega_{20} \Leftrightarrow \omega_{p1}$ in (33), $\omega_{30} \Leftrightarrow \omega_{p3}$ in (34), and the dephasing dip at $\omega_{21} \Leftrightarrow \omega_{p'2}$ in (36). Since in figures 4–6 the qubit–HO coupling is small ($g = 0.18\Delta \ll \Delta, \Omega$), the expressions for ω_{p1}, ω_{p2} and $\omega_{p'2}$ can be written in simpler approximate forms, as: for on resonance in figure 5, $\omega_{10} \Leftrightarrow \omega_{p2}$ and $\omega_{20} \Leftrightarrow \omega_{p1}$ in (40), $\omega_{21} \Leftrightarrow \omega_{p'2}$ in (41); for off resonance in figures 4 and 6. $\omega_{10} \Leftrightarrow \omega_{p2}$ and $\omega_{20} \Leftrightarrow \omega_{p1}$ relate to the renormalized energy difference of the qubit in (42) and to the energy of the HO in (43), $\omega_{21} \Leftrightarrow \omega_{p'2}$ relates to the energy difference of the qubit and the HO in (44).

In [20] by VVBM, four dominant frequencies are presented: one relaxation dip (at $\omega = 0$), one dephasing dip (ω'_{21}) and two dephasing peaks (ω'_{10}, ω'_{20}), and a similar result is also claimed by QUAPI in [19] (see its figure 7). In order to distinguish the dominant frequencies by different methods and/or under different conditions, analogous symbols ω'_{ij} denoting the dominant frequencies of numerical results by VVBM in [20] are employed. As comparison, neither [19] nor [20] presents the dephasing peak (or dip) at ω_{30}, and to our knowledge, it has not been shown in the literature. In all the three figures, the width and height of the dephasing peak at ω_{20} matches quite well with the one at ω'_{20}, but our dephasing peak at ω_{10} and dephasing dip at ω_{21} are much higher and sharper, especially for the on resonance case in figure 5. Meanwhile, the dominant frequencies ω'_{ij} are nearly equal to the dominant frequencies ω_{ij}, but in detail ω'_{ij} are a bit larger than ω_{ij}. For the on resonance case in figure 5, our dephasing dip at ω_{21} has comparable weight with our dephasing peaks at ω_{10} and ω_{20}, which is qualitatively different from the ones by VVBM. As a brief summary, our dynamics and spectra have shown agreement with [20].

As an additional proof, from figures 4 to 6, we have calculated the dynamics $P(t)$ by QUAPI at zero temperature and the corresponding spectra $S(\omega)$ with numerical Fourier transformation to the dynamics $P(t)$. The spectra have shown agreement qualitatively. As shown in [33] for the biased SBM problem, the long time limit will be true only with large $\Delta k_{\max}$ (e.g. $\Delta k_{\max} = 7, 9$). Due to the restriction of our computation resources, we could not provide stable results by QUAPI, which requires a large memory length $\Delta k_{\max}$ and $M \geqslant 6$ (our quantum system is a rather complicated qubit–HO system, not just a TLS in the SBM as shown in [33]). However, the presented dynamics by QUAPI have shown that the tendencies of the long time limit, from Markovian ($\Delta k_{\max} = 1$) cases to the larger memory time ($\Delta k_{\max} = 2, 3$) cases, go closer to the ones of our non-Markovian analytical dynamics.

In order to compare our approach with VVBM in [20], g is kept rather small in figures 4–6, as are the corresponding α (all $\alpha < 0.005$). Nevertheless, our approach has no direct restriction in g and it can work with stronger α. Therefore, in
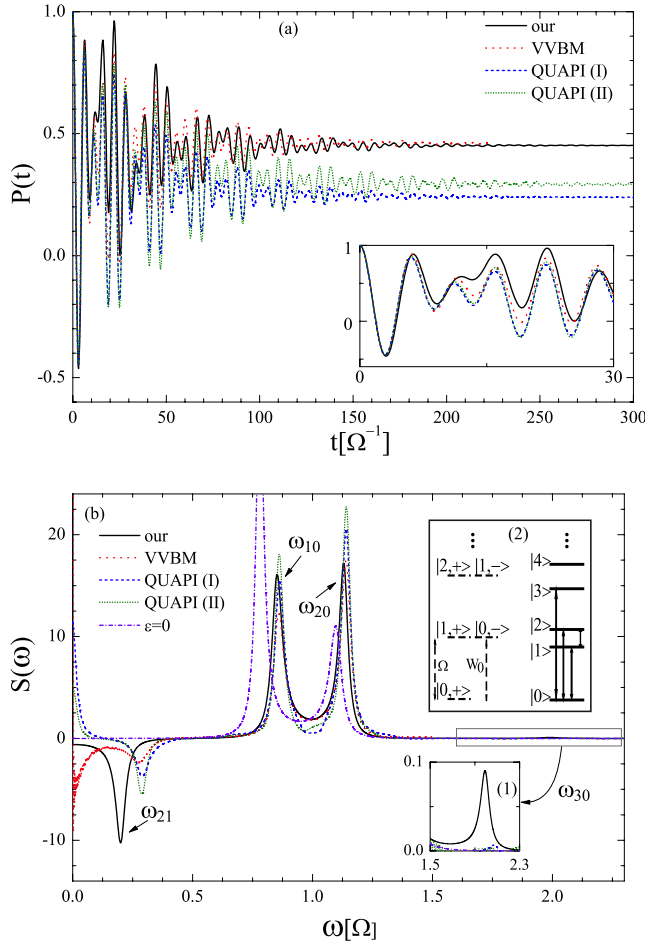
Figure 5. For on resonance $\Omega = W_0 = \sqrt{\Delta^2 + \epsilon^2}$ with $\epsilon = -0.5\Delta$, (a) non-Markovian dynamics $P(t)$ and (b) its corresponding spectrum $S(\omega)$ at zero temperature shows qualitative agreement with VVBM [20] at low temperature $T = 0.1\Delta$,. Similarly to figure 4, our spectrum presents five dominant frequencies ($\omega = 0$, ω_{10}, ω_{20}, ω_{21}, ω_{30}). Our dephasing dip at ω_{21} is much deeper and sharper than the ones by VVBM. Our dip at ω_{21} has a comparable weight to our dephasing peaks at ω_{10} and ω_{20}, which is qualitatively different from the ones by VVBM. For zero bias, there are only two dephasing peaks. Insets: the inset in (a) and inset (1) in (b) present magnified views. Inset (2) in (b) presents the schematic energy levels of the qubit–HO system with finite bias, where the left dashed lines are for the uncoupled case and the right solid lines are for the coupled case. Our dominant frequencies are related to the energy differences of the coupled qubit–HO system with numerical calculation. Parameters: $g = 0.18\Delta$, $\Gamma = 0.0154$, $\alpha = 0.003\,19$. As an additional proof, the results by QUAPI at zero temperature are also provided with parameters for QUAPI (I), $\Delta k_{max} = 1$, $\Delta t = 0.4/\Delta$, $N_d = 100$, $M = 30$ and for QUAPI (II), $\Delta k_{max} = 3$, $\Delta t = 0.4/\Delta$, $N_d = 100$, $M = 6$. However, they are not stable results due to the restriction of our computation resources. With a larger memory length Δk_{max} and a larger sub-space dimension of the qubit–HO system M, QUAPI will provide more stable results.

Figure 6. For off resonance $\Omega = 0.9\Delta$ with $\epsilon = -0.5\Delta$, (a) non-Markovian dynamics $P(t)$ and (b) its corresponding spectrum $S(\omega)$ at zero temperature shows qualitative agreement with VVBM [20] at low temperature $T = 0.1\Delta$. Similarly to figure 4, our spectrum presents five dominant frequencies ($\omega = 0$, ω_{10}, ω_{20}, ω_{21}, ω_{30}). Moreover, our peaks (or dips) are a bit sharper and higher than the ones by VVBM. For zero bias, there are only two dephasing peaks. Insets: the inset in (a) and inset (1) in (b) presents magnified views. Inset (2) in (b) presents the schematic energy levels of the qubit–HO system with finite bias, where the left dashed lines are for the uncoupled case and the right solid lines are for the coupled case. Our dominant frequencies are related to the energy differences of the coupled qubit–HO system with numerical calculation. Parameters: $g = 0.18\Delta$, $\Gamma = 0.0154$, $\alpha = 0.004\,93$. As an additional proof, the results by QUAPI at zero temperature are also provided with parameters for QUAPI (I), $\Delta k_{max} = 1$, $\Delta t = 0.4/\Delta$, $N_d = 100$, $M = 30$; for QUAPI (II), $\Delta k_{max} = 2$, $\Delta t = 0.4/\Delta$, $N_d = 100$, $M = 8$.

figures 7 and 8, it presents a larger qubit–HO coupling ($g = 0.7906\Omega$) and larger spin–bath coupling ($\alpha = 0.01, 0.05, 0.1$) for positive detunings ($\Omega = 2\Delta > W_0$) and near resonance ($\Omega = \Delta \sim W_0$). The results for negative detunings are similar to the positive ones and the figure for negative detunings is not repeated. Likewise, the biased spectrum presents one
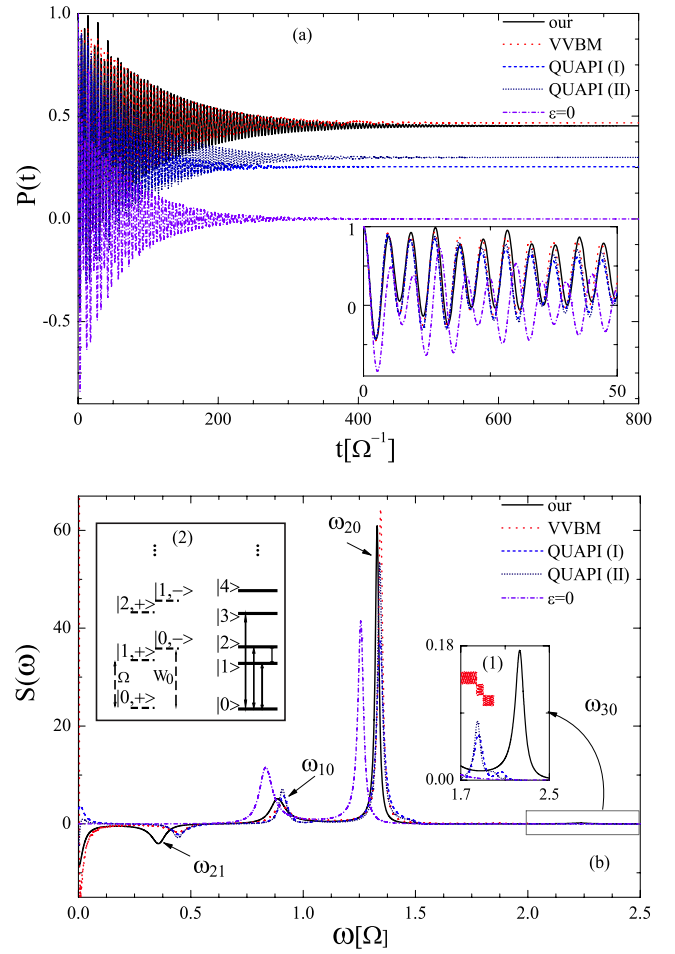
relaxation peak (at $\omega = 0$) and four dephasing peaks (ω_{10}, ω_{20}, ω_{21}, ω_{30}). The dominant frequencies can be interpreted well with the energy differences of the four lowest energy levels of the coupled qubit–HO system as above. Similarly, they can also be interpreted well with the relaxation peak at $\omega = 0 \Leftrightarrow \omega_{p'1} = 0$ in (35), the dephasing peaks at $\omega_{10} \Leftrightarrow \omega_{p2}$ and $\omega_{20} \Leftrightarrow \omega_{p1}$ in (33), $\omega_{30} \Leftrightarrow \omega_{p3}$ in (34), and the dephasing dip at $\omega_{21} \Leftrightarrow \omega_{p'2}$ in (36). In contrast to the small qubit–HO coupling, the weights of the dephasing peaks at ω_{30} shown in figures 7 and 8 grow larger. For near resonance in figure 8, our
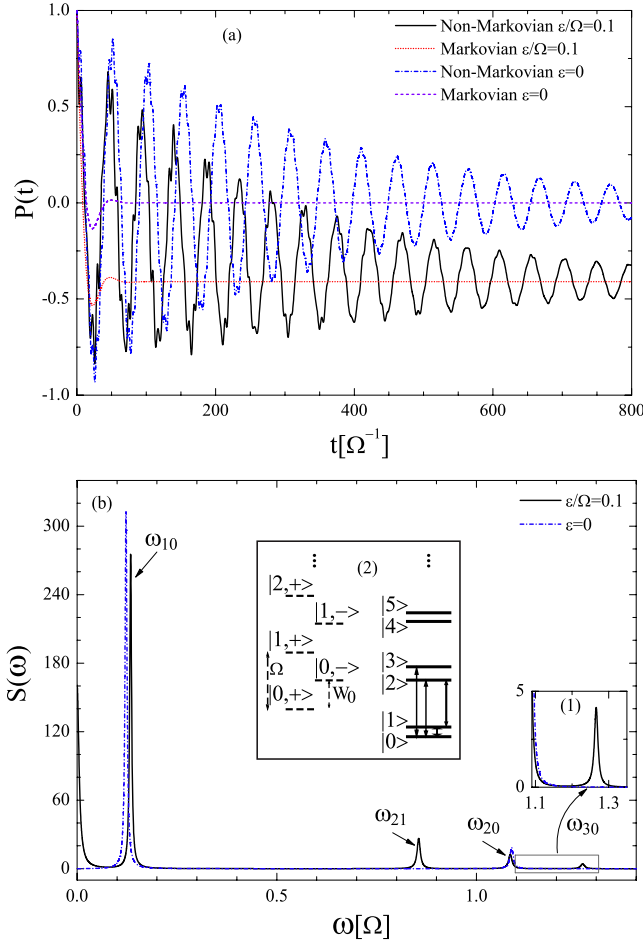
Figure 7. For off resonance $\Delta = 0.5\Omega$ with larger qubit–HO coupling $g = 0.7906\Omega$, (a) non-Markovian dynamics $P(t)$ and (b) its corresponding spectrum $S(\omega)$ at zero temperature are shown with bias $\epsilon = 0.1\Omega$ and with zero bias, while the Markovian one in (a) has shown the long time limit. Similarly, the biased spectrum presents four dephasing peaks ($\omega_{10}, \omega_{20}, \omega_{21}, \omega_{30}$) and one relaxation peak ($\omega = 0$), while the unbiased one only presents two dephasing peaks. Insets: inset (1) in (b) presents a magnified view. Inset (2) in (b) presents the schematic energy levels of the qubit–HO system with finite bias, where the left dashed lines are for the uncoupled case and the right solid lines are for the coupled case. Our dominant frequencies are related to the energy differences of the coupled qubit–HO system with numerical calculation. Parameters: $\alpha = 0.01$, $\Gamma = 0.002$.

dephasing peak at ω_{21} has comparable weight to our dephasing peaks at ω_{10} and ω_{20} and the weight of the dephasing peak at ω_{30} grows much larger than that for off resonance in figure 7.

Meanwhile, the corresponding Markovian dynamics given by (48) have been presented in figure 7 to show the long time limit. Moreover, in figure 8 with the same $\Delta = \Omega$, $g = 0.7906\Omega$ and $\epsilon = 0.1\Omega$, the effect with different Γ (=0.002, 0.01, 0.02) is shown, as well as different corresponding α (=0.01, 0.05, 0.1). The results show that the distributions of the dominant frequencies vary little, but with smaller Γ or α, the dephasing peaks will be higher and sharper and the dephasing will be smaller, which is physically reasonable.

The non-Markovian dynamics and the spectra for zero bias ($\epsilon = 0$) in figures 3–8 have shown that the spectra have only presented two dephasing peaks ($\omega''_{10}, \omega''_{20}$) for zero bias,
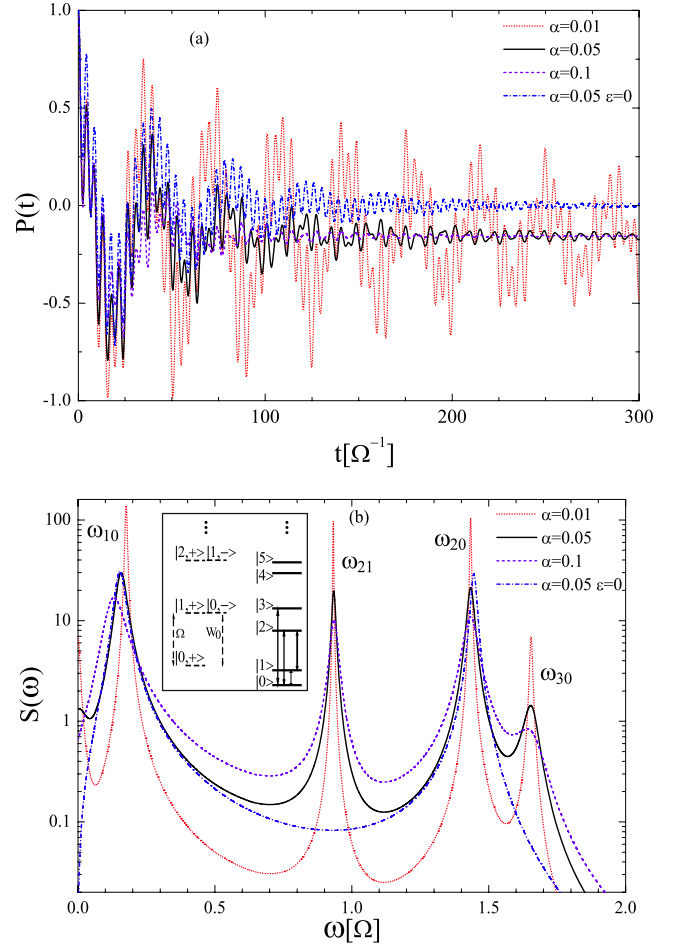
Figure 8. For near resonance $\Delta = \Omega$ with larger qubit–HO coupling $g = 0.7906\Omega$, (a) non-Markovian dynamics $P(t)$ and (b) its corresponding spectrum $S(\omega)$ at zero temperature are compared between the biased case $\epsilon = 0.1\Omega$ and the unbiased case at $\alpha = 0.05$, $\Gamma = 0.01$. Similarly, the biased spectrum presents four dephasing peaks ($\omega_{10}, \omega_{20}, \omega_{21}, \omega_{30}$) and one relaxation peak ($\omega = 0$), while the unbiased one only presents two dephasing peaks. In addition, with the same $\Delta = \Omega$, $g = 0.7906\Omega$ and $\epsilon = 0.1\Omega$, the effect with different Γ or α (red dot line: $\alpha = 0.01$, $\Gamma = 0.002$ and violet dash line: $\alpha = 0.1$, $\Gamma = 0.02$) is shown: the distributions of the dominant frequencies vary little, but with smaller Γ or α, the dephasing peaks will be higher and sharper and the dephasing will be smaller. Insets: inset in (b) presents the schematic energy levels of the qubit–HO system with finite bias where the left dashed lines are for the uncoupled case and the right solid lines are for the coupled case. Our dominant frequencies are related to the energy differences of the coupled qubit–HO system with numerical calculation.

which are consistent with the literature results and have been interpreted in two ways, as shown above (with (38) or the selection rules). Similarly, ω''_{ij} has been employed to denote the dominant frequencies for zero bias and they are related to the energy levels of the unbiased coupled qubit–HO system. Compared to zero bias, the effect of non-zero bias is shown in figures 4–8, i.e., three additional resonant peaks appear in the spectrum: the relaxation peak at $\omega = 0$, a third dephasing peak (dip) at ω_{21} and a fourth dephasing peak at ω_{30}. Note that the frequency ω''_{10} for zero bias is usually smaller than the biased one ω_{10}.
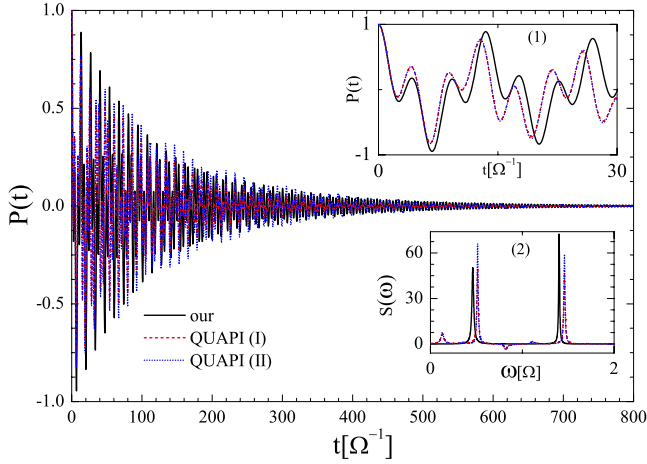
Figure 9. As a proof, a comparison between our non-Markovian dynamics $P(t)$ and the numerical results by QUAPI at zero temperature with moderately strong qubit–HO coupling $g = 0.5\Delta$, for the near resonance case $\Delta = \Omega$ with $\epsilon = 0$. Both the dynamics and the spectra show rough qualitative agreement, where the results by QUAPI are restricted by our computation resources from reaching stable results. Parameters for QUAPI (I), $\Delta k_{max} = 1$, $\Delta t = 0.5/\Delta$, $N_d = 100$, $M = 30$; for QUAPI (II), $\Delta k_{max} = 2$, $\Delta t = 0.5/\Delta$, $N_d = 100$, $M = 10$. Parameters: $g = 0.5\Delta$, $\Gamma = 0.005$, $\alpha = 0.01$.
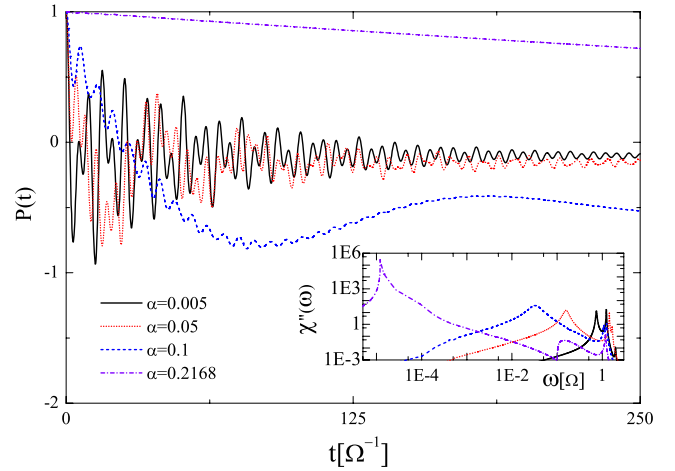
Figure 10. Non-Markovian dynamics $P(t)$ for the near resonance case $\Delta = \Omega$ with $\epsilon = 0.1\Omega$ and $\Gamma = 0.01$ for different spin–bath coupling $\alpha = 0.005, 0.05, 0.1, 0.2168$ (corresponding qubit–HO coupling $g/\Omega = 0.25, 0.7906, 1.1180, 1.6462$) all with $\alpha < \alpha_c = 0.216\,832\,29$. It shows that when increasing α from weak to strong, the dynamics go from abundant oscillation to nearly pure damping. Insets: the inset is the susceptibility $\chi''(\omega)$ versus ω and it shows that when increasing α close to α_c the highest peak goes close to infinity near $\omega = 0$.

For non-zero bias, at $\omega = 0$ and ω_{21}, two dips are clearly shown for negative bias and two peaks instead for positive bias in figures 4–8. It can be interpreted as follows: $\omega = 0$ is mapped to $\omega_{p'1} = 0$ and ω_{21} is mapped to $\omega_{p'2}$; $\omega_{p'1}$ and $\omega_{p'2}$ are the solutions $\omega_{p'}$ of equation (31); equation (31) is from the first term of $S(\omega)$ in (29); the sign of the first term of $S(\omega)$ in (29) is the same as the bias ϵ. Similar analysis can be done for the remaining three dominant frequencies. Therefore, there are always peaks at ω_{10}, ω_{20} and ω_{30}; while at $\omega = 0$ and ω_{21}, there are peaks for positive bias ($\epsilon > 0$) and dips for negative bias ($\epsilon < 0$).

In figure 9, as an additional proof for our result for the larger qubit–HO coupling, we have made comparisons between our non-Markovian dynamics $P(t)$ and the numerical results by QUAPI ($\Delta k_{max} = 1, 2$) at zero temperature, as well as the spectra. Similarly, due to the restriction of our computation resources, we have only presented parameters as shown in figure 9 and we could not provide stable results by QUAPI, which requires a large memory length Δk_{max} (as shown in figure 2 for SBM in [33], $\Delta k_{max} = 5, 7$) and $M \geqslant 6$. However, the comparison shows qualitative agreement in figure 9: the dominant frequencies are close; the dynamics have similar patterns.

As a brief summary to the biased spectrum $S(\omega)$ of the non-Markovian dynamics $P(t)$: there are five resonances, i.e., the relaxation peak (dip) at $\omega = 0$, one dephasing peak (dip) at $\omega = \omega_{21}$, three dephasing peaks at $\omega = \omega_{10}, \omega_{20}, \omega_{30}$, which are related to the energy differences of the four lowest energy levels of the coupled qubit–HO system. For the qubit having the HO at positive detunings ($\Omega > W_0$), the dephasing peak at $\omega = \omega_{10}$ and the relaxation peak (dip) at $\omega = 0$ are generally dominant; for on/near resonance ($\Omega \cong W_0$), the dephasing peaks (dip) at $\omega = \omega_{10}, \omega_{20}, \omega_{21}$ are generally dominant; for

negative detunings ($\Omega < W_0$), if g is small, the dephasing peak at $\omega = \omega_{20}$ is generally dominant, otherwise, the peak at $\omega = \omega_{10}$ is dominant. A rough idea is that: the dominant frequency(ies) closer to the renormalized energy difference of the qubit (W_0) usually contribute(s) more weight.

Figure 10 shows the dynamics with different α for non-zero bias. As usual, larger decay accompanies larger α. Our method also works well for sufficiently strong spin–bath coupling as long as $\alpha < \alpha_c$ (see section 5) beyond weak coupling regime.

The sum rule of the non-Markovian dynamics is checked, as shown in table 1, and it is exactly satisfied with representative parameters for $\alpha < \alpha_c$.

5. Susceptibility and coherent–incoherent transition

The susceptibility $\chi(\omega) = -G(\omega)$, where $G(\omega)$ (obtained in the appendix in detail) is the Fourier transformation of the retarded Green function $G(t) = -i\theta(t)Z^{-1}\text{Tr}\{\exp(-\beta H) [\sigma_z(t), \sigma_z]\}$, in which $\theta(t)$ is the unit step function. The imaginary part of $\chi(\omega)$ is $\chi''(\omega)$,

$$\chi''(\omega) = \frac{\eta^2 \Delta^2}{W^2} \left\{ \frac{\Gamma(\omega)\theta(\omega)}{[\omega - W - \Sigma(\omega)]^2 + \Gamma^2(\omega)} - \frac{\Gamma(-\omega)\theta(-\omega)}{[\omega + W + \Sigma(-\omega)]^2 + \Gamma^2(-\omega)} \right\}, \quad (49)$$

and its real part $\chi'(\omega = 0)$ can be obtained by the Kramers–Kronig relation as

$$\chi'(\omega = 0) = \frac{2}{\pi} \int_0^\infty \frac{\chi''(\omega)}{\omega} \, d\omega. \quad (50)$$

Table 1. The sum rule and the Shiba relation are checked with representative parameters. Here $R \equiv \lim_{\omega \to 0} F(\omega) / \frac{\pi}{4} [\chi'(0)]^2$, where $F(\omega) = \chi''(\omega)/J(\omega)$.

α	Δ/Ω	Γ	ϵ/Ω	$\chi'(0)$	$\lim_{\omega \to 0} F(\omega)$	R	$P(t=0)$
0.1	0.1	0.05	0.1	5.897 376 962	27.315 405 94	1	1
0.1	0.2	0.05	0.1	10.161 505 27	81.097 221 54	1	1
0.1	0.5	0.01	0	77.385 195 88	4703.332 194	1	1
0.3	0.5	0.01	0.01	0.058 457 193 99	0.002 683 896 792	1	1
0.1	0.5	0.1	0.5	1.558 179 498	1.906 886 539	1	1
0.2	0.5	0.2	0.1	5.784 656 542	26.281 190 72	1	1
0.1	1	0.01	0	49.762 408 45	1944.879 348	1	1
0.3	1	0.01	0.01	0.233 784 401	0.042 926 051 41	1	1
0.1	1	0.01	0.1	36.237 221 91	1031.3348	1	1
0.21	1	0.01	0.1	7.819 123 532	48.018 217 04	0.999 999 9999	1
0.216	1	0.01	0.1	49.367 629 68	1914.143 282	1.000 000 025	1
0.2168	1	0.01	0.1	1228.943 521	1186 131.33	0.999 951 7554	0.999 999 9947
0.2	1	0.05	0.01	7.857 533 292	48.491 134 04	1	1
0.5	1	0.2	0.1	5.312 073 901	22.162 4668	1	1
0.1	1.1	0.05	0.1	2.920 164 619	6.697 373 981	1	1
0.2	1.2	0.01	0.1	7.494 084 145	44.108 979 66	1	1
0.1	1.5	0.05	0.1	2.003 650 314	3.153 070 92	1	1

Our approach can be checked by the Shiba relation [35–38]

$$\lim_{\omega \to 0} \frac{\chi''(\omega)}{J(\omega)} = \frac{\pi}{4} [\chi'(\omega = 0)]^2. \tag{51}$$

As long as $\alpha < \alpha_c$, the Shiba relation is exactly satisfied, as shown in table 1 with representative parameters.

The susceptibility $\chi''(\omega)$ is the same as the second term of $S(\omega)$ in (29) for $\omega \geqslant 0$ and it is an odd function of ω. Usually $\chi''(\omega = 0) = 0$. On increasing α to a particular value α_c, a critical phase occurs and $\chi''(\omega = 0) = \infty$. Meanwhile, $\Gamma(\omega) \propto \omega$ and we have checked that $[\omega - W - \Sigma(\omega)] \propto \omega$ when $\omega \to 0$. Thus, the coherent–incoherent transition point [1, 2] α_c is defined as the solution of

$$- W - \Sigma(0) = 0. \tag{52}$$

In figure 10, non-Markovian dynamics $P(t)$ and the susceptibilities $\chi''(\omega)$ have been shown with different α (=0.005, 0.05, 0.1, 0.2168). In addition, the coherent–incoherent transition point α_c (=0.216 832 29) is calculated by (52). $P(t)$ exhibits considerable oscillation for weak α (=0.005), beating oscillation for moderate α (=0.05), badly damped oscillation for moderately strong α (=0.1), and nearly pure damping for sufficiently strong α (=0.2168) (nearly equals to α_c). In the inset of figure 10, $\chi''(\omega)$ is plotted against ω, and the curve shows three non-zero frequency peaks for all $\alpha < \alpha_c$. Increasing α from weak (0.005) to strong (0.2168), the peak at the smallest frequency rapidly moves close to $\omega = 0$ and the corresponding peak grows to a large value, while the other peaks approach zero. When $\alpha < \alpha_c$, $\chi''(\omega = 0) = 0$. At $\alpha = \alpha_c$, $\chi''(\omega = 0) = \infty$. Therefore, the particular value α_c is the coherent–incoherent transition point.

In figure 11, phase diagrams of the coherent–incoherent transition point α_c versus bias ϵ with different Γ are shown. The area for $\alpha < \alpha_c$ is called the 'coherent phase', and for $\alpha > \alpha_c$ the 'incoherent phase'. As shown in figure 11(a) for near resonance $\Delta = \Omega$, the changing curve of α_c versus

ϵ is an ohmic-like. α_c gradually increases with increasing bias, and it increases rapidly with increasing Γ. As shown in figure 11(b) for off resonance $\Delta = 0.5\Omega$, the changing curve is nontrivial for small $\Gamma = 0.075$: one sharp peak exists around $\epsilon = 0.0655\Omega$ and the curve at the ends behaves ohmic-like. The sharp peak is substituted by a smooth kink for $\Gamma = 0.0762$. While for $\Gamma = 0.08, 0.1$, the kink disappears and the whole curve behaves ohmic-like. Further results show that when decreasing Γ (e.g. $\Gamma < 0.075$) the sharp peak grows much sharper and higher, and the corresponding bias of the peak becomes smaller. Under smaller Γ, a significant difference of α_c between the steep area at finite bias and the platform area with zero bias might be utilized, e.g. for reading out the qubit state.

6. Conclusions

We have investigated the biased SBM with a Lorentzian spectral density by a new analytical approach at zero temperature. An equivalent description of the system is provided by a biased qubit coupled through a HO to an ohmic environment. The starting point is the general SBM Hamiltonian (2) without RWA. We have applied two unitary transformations to the Hamiltonian and the non-Markovian master equation within the nontrivial Born approximation to get an expression for the density operator. With the density operator, we have provided analytical expressions for the non-Markovian dynamics $P(t)$ and the corresponding spectrum $S(\omega)$. Meanwhile, the localized–delocalized transition point α_L and the coherent–incoherent transition point α_c are determined, which have not been provided so far (except α_c with zero bias by [26]), as well as the analytical ground energy, the renormalized tunneling factor η and the susceptibility $\chi''(\omega)$. The sum rule and the Shiba relation are carefully checked, and they are exactly satisfied as long as $\alpha < \alpha_c$.

The biased dynamics and the corresponding spectrum are key topics in this paper. Both for biased and unbiased cases, they have been compared with the results of other groups and
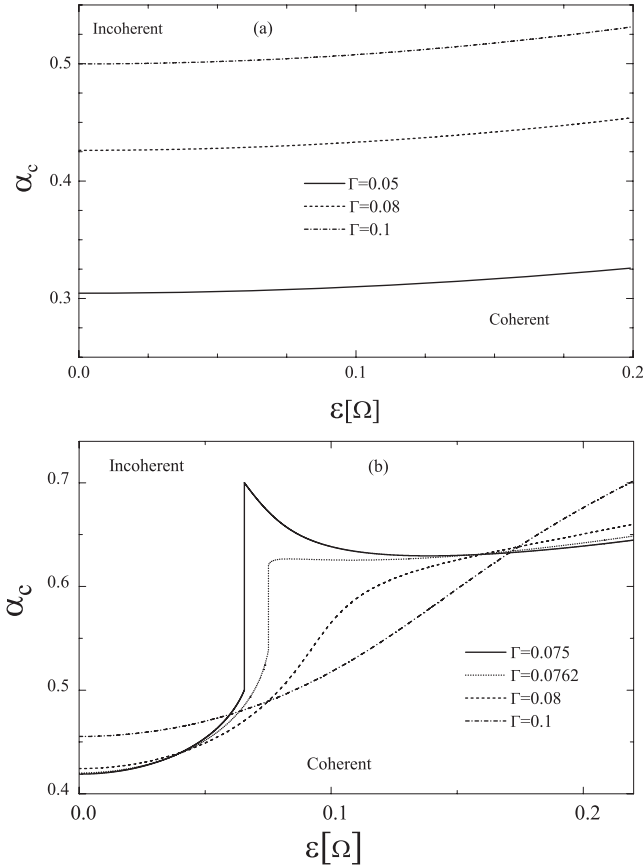
Figure 11. Phase diagram of the coherent–incoherent transition point α_c versus bias ϵ, for (a) near resonance $\Delta = \Omega$ with different $\Gamma = 0.05, 0.08, 0.1$; (b) off resonance $\Delta = 0.5\Omega$ with different $\Gamma = 0.075, 0.0762, 0.08, 0.1$. A kink appears when Γ is small for off resonance, otherwise α_c gradually increases with ϵ.

have shown good agreement. For non-zero bias, our spectrum presents *five dominant frequencies*: the relaxation peak (dip) at $\omega = 0$, one dephasing peak (dip) at $\omega = \omega_{21}$ and three dephasing peaks at $\omega = \omega_{10}, \omega_{20}, \omega_{30}$. Our approach has no direct restriction on the qubit–HO coupling g. Therefore, it is a good way to investigate the dynamics in the little-studied strong qubit–HO coupling regime, especially in the static biased case, which has not been studied yet to our knowledge, as shown in figures 7, 8 and 10. As an additional proof, but restricted by our computational resources ($\Delta k_{max} = 3$ and $M \geqslant 6$), we have obtained results by QUAPI with zero bias for weak or sufficient strong qubit–HO coupling ($g = 0.18\Delta$ in figure 3 and $g = 0.5\Delta$ in figure 9) and non-zero bias (from figures 4 to 6), and the dynamics and the spectra have shown agreement qualitatively, but the stable dynamics for non-zero bias are still beyond our computational resources. Moreover, the origin and the meanings of the dominant frequencies have been studied in two ways: providing analytical expressions for each dominant frequency with small HO–environment coupling Γ and comparing them with the spectra of the qubit–HO systems. We have also discussed why there are sometimes peaks and sometimes dips, as well as the weight distribution of the peaks (dips) and why there are only two dominant frequencies for the unbiased case. Meanwhile, fixing other

parameters, the effects with different α and corresponding Γ are also shown. The dynamics at the long time limit are given analytically as $-\epsilon/W$, which are consistent with Markovian dynamics.

In summary, we have provided analytical results for interesting physical quantities without the Markovian approximation and our approach works well at arbitrary detunings: on/off resonance, with/without bias and from weak to sufficiently strong spin–bath coupling as long as $\alpha < \alpha_c$. Admittedly, this approach is not suitable for very strong spin–bath coupling, e.g. $\alpha > \alpha_c$. Nevertheless, the coherent regime is the most interesting one in the field of quantum computation and quantum information.

Acknowledgments

Appendix

Following the transformation made to H to reach $\tilde{H}$, the retarded Green function is

$$
\begin{aligned}
G(t) &= -\mathrm{i}\theta(t)Z^{-1}\mathrm{Tr}\{\exp(-\beta H) \\
&\quad \times [\exp(\mathrm{i}Ht)\sigma_z \exp(-\mathrm{i}Ht), \sigma_z]\} \\
&= -\mathrm{i}\theta(t)Z^{-1}\mathrm{Tr}\bigg\{\exp(-\beta\tilde{H}) \\
&\quad \times \bigg(\frac{\epsilon^2}{W^2}[\tilde{\sigma}_z(t), \tilde{\sigma}_z] + \frac{\eta^2\Delta^2}{W^2}[\tilde{\sigma}_x(t), \tilde{\sigma}_x] \\
&\quad - \frac{\eta\Delta\epsilon}{W^2}[\tilde{\sigma}_z(t), \tilde{\sigma}_x] - \frac{\eta\Delta\epsilon}{W^2}[\tilde{\sigma}_x(t), \tilde{\sigma}_z]\bigg)\bigg\}.
\end{aligned} \tag{A.1}
$$

The Fourier transformation of $G(t)$ is denoted as

$$
\begin{aligned}
G(\omega) &= \frac{\epsilon^2}{W^2}\langle\langle\tilde{\sigma}_z; \tilde{\sigma}_z\rangle\rangle + \frac{\eta^2\Delta^2}{W^2}\langle\langle\tilde{\sigma}_x; \tilde{\sigma}_x\rangle\rangle \\
&\quad - \frac{\eta\Delta\epsilon}{W^2}\langle\langle\tilde{\sigma}_z; \tilde{\sigma}_x\rangle\rangle - \frac{\eta\Delta\epsilon}{W^2}\langle\langle\tilde{\sigma}_x; \tilde{\sigma}_z\rangle\rangle,
\end{aligned} \tag{A.2}
$$

where

$$
\begin{aligned}
\langle\langle A; B\rangle\rangle &= -\mathrm{i}\theta(t)Z^{-1} \\
&\quad \times \mathrm{Tr}\{\exp(-\beta\tilde{H})[\exp(\mathrm{i}\tilde{H}t)A\exp(-\mathrm{i}\tilde{H}t), B]\}
\end{aligned}
$$

denotes the retarded Green function which satisfies the following equation of motion,

$$
\omega\langle\langle A; B\rangle\rangle = \langle[A, B]\rangle + \langle\langle[A, \tilde{H}]; B\rangle\rangle,
$$

$$
\langle[A, B]\rangle = Z^{-1}\mathrm{Tr}\{\exp(-\beta\tilde{H})[A, B]\}.
$$

Thus, we can get the following equation chain:

$$
\begin{aligned}
\omega\langle\langle\tilde{\sigma}_x; \tilde{\sigma}_x\rangle\rangle &= W\langle\langle\mathrm{i}\tilde{\sigma}_y; \tilde{\sigma}_x\rangle\rangle \\
&\quad + \sum_k Q_k\langle\langle\mathrm{i}\tilde{\sigma}_y(b_k^\dagger + b_k); \tilde{\sigma}_x\rangle\rangle \\
&\quad - \sum_k V_k\langle\langle\tilde{\sigma}_z(b_k^\dagger - b_k); \tilde{\sigma}_x\rangle\rangle,
\end{aligned} \tag{A.3}
$$

$$\omega\langle\langle i\tilde{\sigma}_y;\tilde{\sigma}_x\rangle\rangle = 2\langle\tilde{\sigma}_z\rangle_{\tilde{H}_0} + W\langle\langle\tilde{\sigma}_x;\tilde{\sigma}_x\rangle\rangle$$
$$+ \sum_k Q_k\langle\langle\tilde{\sigma}_x(b_k^\dagger + b_k);\tilde{\sigma}_x\rangle\rangle$$
$$+ \sum_k V_k\langle\langle\tilde{\sigma}_z(b_k^\dagger + b_k);\tilde{\sigma}_x\rangle\rangle, \tag{A.4}$$

$$\omega\langle\langle\tilde{\sigma}_x(b_k^\dagger + b_k);\tilde{\sigma}_x\rangle\rangle = -\omega_k\langle\langle\tilde{\sigma}_x(b_k^\dagger - b_k);\tilde{\sigma}_x\rangle\rangle$$
$$+ W\langle\langle i\tilde{\sigma}_y(b_k^\dagger + b_k);\tilde{\sigma}_x\rangle\rangle + Q_k\langle\langle i\tilde{\sigma}_y;\tilde{\sigma}_x\rangle\rangle, \tag{A.5}$$

$$\omega\langle\langle\tilde{\sigma}_x(b_k^\dagger - b_k);\tilde{\sigma}_x\rangle\rangle = -\omega_k\langle\langle\tilde{\sigma}_x(b_k^\dagger + b_k);\tilde{\sigma}_x\rangle\rangle$$
$$+ W\langle\langle i\tilde{\sigma}_y(b_k^\dagger - b_k);\tilde{\sigma}_x\rangle\rangle - Q_k\langle\langle\tilde{\sigma}_x;\tilde{\sigma}_x\rangle\rangle, \tag{A.6}$$

$$\omega\langle\langle i\tilde{\sigma}_y(b_k^\dagger + b_k);\tilde{\sigma}_x\rangle\rangle = -\omega_k\langle\langle i\tilde{\sigma}_y(b_k^\dagger - b_k);\tilde{\sigma}_x\rangle\rangle$$
$$+ W\langle\langle\tilde{\sigma}_x(b_k^\dagger + b_k);\tilde{\sigma}_x\rangle\rangle + Q_k\langle\langle\tilde{\sigma}_x;\tilde{\sigma}_x\rangle\rangle, \tag{A.7}$$

$$\omega\langle\langle i\tilde{\sigma}_y(b_k^\dagger - b_k);\tilde{\sigma}_x\rangle\rangle = -\omega_k\langle\langle i\tilde{\sigma}_y(b_k^\dagger + b_k);\tilde{\sigma}_x\rangle\rangle$$
$$+ W\langle\langle\tilde{\sigma}_x(b_k^\dagger - b_k);\tilde{\sigma}_x\rangle\rangle - Q_k\langle\langle i\tilde{\sigma}_y;\tilde{\sigma}_x\rangle\rangle, \tag{A.8}$$

where $\langle\tilde{\sigma}_z\rangle_{\tilde{H}_0} = \langle g_0|\tilde{\sigma}_z|g_0\rangle = 1$. We have already made the cutoff approximation for the equation chains at the second order of λ_k. In addition, $\langle\langle\tilde{\sigma}_z;\tilde{\sigma}_x\rangle\rangle = 0$, $\langle\langle\tilde{\sigma}_z;\tilde{\sigma}_z\rangle\rangle = 0$, and $\langle\langle\tilde{\sigma}_x;\tilde{\sigma}_z\rangle\rangle = 0$, so the solution for $G(\omega)$ is

$$G(\omega) = \frac{\eta^2\Delta^2}{W^2}$$
$$\times \left(\frac{1}{\omega - W - \sum_k V_k^2/(\omega - \omega_k) - \sum_k Q_k^2/(\omega - W - \omega_k)} \right.$$
$$\left. - \frac{1}{\omega + W - \sum_k V_k^2/(\omega + \omega_k) - \sum_k Q_k^2/(\omega + W + \omega_k)} \right). \tag{A.9}$$

References

[1] Leggett A J, Chakravarty S, Dorsey A T, Fisher M P A, Garg A and Zwerger W 1987 *Rev. Mod. Phys.* **59** 1
[2] Weiss U 1999 *Quantum Dissipative Systems* (Singapore: World Scientific)
[3] Grifoni M and Hänggi P 1998 *Phys. Rep.* **304** 229
[4] Vion D, Aassime A, Cottet A, Joyez P, Pothier H, Urbina C, Esteve D and Devoret M H 2002 *Science* **296** 886
[5] Yu Y, Han S, Chu X, Chu S-I and Wang Z 2002 *Science* **296** 889
[6] Chiorescu I, Nakamura Y, Harmans C J P M and Mooij J E 2003 *Science* **299** 1869
[7] Chiorescu I, Bertet P, Semba K, Nakamura Y, Harmans C J P M and Mooij J E 2004 *Nature* **431** 159
[8] Imamog Lu A, Awschalom D D, Burkard G, DiVincenzo D P, Loss D, Sherwin M and Small A 1999 *Phys. Rev. Lett.* **83** 4204
[9] Martinis J M, Nam S, Aumentado J and Urbina C 2002 *Phys. Rev. Lett.* **89** 117901
[10] Wallraff A, Schuster D I, Blais A, Frunzio L, Huang R S, Majer J, Kumar S, Girvin S M and Schoelkopf R J 2004 *Nature* **431** 162
[11] Thorwart M, Hartmann L, Goychuk I and Hänggi P 2000 *J. Mod. Opt.* **47** 2905
[12] van der Wal C H, ter Haar A C J, Wilhelm F K, Schouten R N, Harmans C J P M, Orlando T P, Lloyd S and Mooij J E 2000 *Science* **290** 773
[13] Garg A, Onuchic J N and Ambegaokar V 1985 *J. Chem. Phys.* **83** 4491
[14] Tian L, Lloyd S and Orlando T P 2002 *Phys. Rev.* B **65** 144516
[15] van der Wal C H, Wilhelm F K, Harmans C J P M and Mooij J E 2003 *Eur. Phys. J.* B **31** 111
[16] Robertson T L, Plourde B L T, Hime T, Linzen S, Reichardt P A, Wilhelm F K and Clarke J 2005 *Phys. Rev.* B **72** 024513
[17] Goorden M C, Thorwart M and Grifoni M 2004 *Phys. Rev. Lett.* **93** 267005
[18] Goorden M C, Thorwart M and Grifoni M 2005 *Eur. Phys. J.* B **45** 405–17
[19] Thorwart M, Paladino E and Grifoni M 2004 *Chem. Phys.* **296** 333
[20] Hausinger J and Grifoni M 2008 *New J. Phys.* **10** 115015
[21] Kleff S, Kehrein S and von Delft J 2003 *Physica* E **18** 343
[22] Wilhelm F K, Kleff S and von Delft J 2004 *Chem. Phys.* **296** 345
[23] Kleff S, Kehrein S and von Delft J 2004 *Phys. Rev.* B **70** 014516
[24] Nesi F, Grifoni M and Paladino E 2007 *New J. Phys.* **9** 316
[25] Brito F and Caldeira A O 2008 *New J. Phys.* **10** 115014
[26] Huang P H and Zheng H 2008 *J. Phys.: Condens. Matter* **20** 395233
[27] Stauber T and Mielke A 2003 *J. Phys. A: Math. Gen.* **36** 2707–36
[28] Zheng H 2004 *Eur. Phys. J.* B **38** 559
[29] Burkard G 2009 *Phys. Rev.* B **79** 125317
[30] DiVincenzo D P and Loss D 2005 *Phys. Rev.* B **71** 035318
[31] Jaynes E T and Cummings F W 1963 *Proc. IEEE* **51** 89
[32] Makri N 1995 *J. Math. Phys.* **36** 2430
[33] Makri N and Makarov D E 1995 *J. Chem. Phys.* **102** 4600
[34] Makri N and Makarov D E 1995 *J. Chem. Phys.* **102** 4611
[35] Sassetti M and Weiss U 1990 *Phys. Rev.* A **41** 5383
[36] Sassetti M and Weiss U 1990 *Phys. Rev. Lett.* **65** 2262
[37] Costi T A and Kieffer C 1996 *Phys. Rev. Lett.* **76** 1683
[38] Costi T A 1998 *Phys. Rev. Lett.* **80** 1038